Shafranov shift bifurcation of turbulent transport in the high β_p scenario on DIII-D

J. McClenaghan[1], A.M. Garofalo[2], G.M. Staebler[2], S.Y. Ding[3], X. Gong[3], and J. Qian[3]

[1]Oak Ridge Associated Universities, Oak Ridge, TN 37831, USA

[2]General Atomics, PO Box 85608, San Diego, CA 92186–5608, USA

[3]Institute of Plasma Physics, Chinese Academy of Sciences, Hefei 230031, People's Republic of China

May 30, 2018

Abstract

Shafranov shift stabilization of turbulence creates a bifurcation in transport, leading to multiple confinement states in the high β_p scenario on DIII-D: An H-mode confinement state with a high edge pedestal, and a higher confinement state with a low pedestal and an internal transport barrier (ITB). The bifurcation is observed experimentally in the ion energy transport with respect to mid-radius ($\rho = 0.6$) pressure gradient. Here, we propose a mechanism for the often observed spontaneous transition between states and formation of an ITB at fixed β_N. The high pedestal results in the plasma at large radius ($\rho = 0.8$) being in a second stability region with respect to KBMs, while the low pedestal leads to plasma in first stability at large radius. To access the high confinement state, the large radius transitions from the second stability to the first stability state. Transient perturbations such as ELMs can trigger the transition between states by temporarily reducing the KBM drive.

Understanding the Shafranov shift stabilization of turbulence is critical for a fusion reactor, since other forms of turbulence stabilization, such as ExB rotation shear are thought to scale poorly with reactor size

[1]. Interplay between the Shafranov shift and magnetic shear has been theoretically shown to reduce peak growth rates of low-k turbulence when $\alpha - s > 0$ for a circular flux surface equilibrium [2], where $\alpha \propto \partial p/\partial \rho$ is a measure of Shafranov shift and s is the magnetic shear. This reduction of turbulence from the Shafranov shift was thought to play an important role in formation of ITBs in plasmas with large negative central shear due to the large negative value of s [3]. However, later work suggested that the interplay between magnetic shear and Shafranov shift alone was not capable of sustaining the enhanced confinement in the large negative central shear scenario [4].

High β_p operation [5, 6, 7] is advantageous for a fusion reactor as it reduces the requirement on external current drive. In the high β_p scenario on DIII-D, ion energy transport is reduced to neoclassical levels in the core resulting in formation of a large radius ITB in all transport channels [8]. The high β_p scenario has a high bootstrap fraction (f_{bs}), which creates multiple channels for positive feedback of turbulence suppression. This high bootstrap fraction naturally aligns the current profile and the pressure profile, since the bootstrap current is generated from the pressure gradient. Thus, an increase in pressure gradient increases α and decreases s simultaneously, both of which can further suppress turbulence. Recent modeling work has suggested that the resulting ITB is consistent with the plasma being on the second stability with respect to the kinetic ballooning mode (KBM), or over the "KBM mountain" [9].

In this letter, a bifurcation is observed in the experimental ion energy transport with respect to mid-radius pressure gradient. An edge localized mode (ELM) is proposed as a mechanism for the often observed spontaneous transition between states and formation of an ITB. The reduced gyro-Landau fluid code TGLF is used to analyze the turbulent transport of different confinement states in the high β_p scenario. TGLF has successfully predicted the ion energy transport in high β_p plasmas [8]. The model solves for linear eigenmodes of ion and electron temperature gradient modes (ITG, ETG), trapped electron modes, and electromagnetic kinetic ballooning modes (KBM) [10]. TGLF uses the linear growth rates to make a quasi-linear prediction of the energy fluxes with the quasi-linear weights determined by fitting to nonlinear gyrokinetic GYRO [11] simulations.

In the DIII-D high β_p discharge shown in Figure 1, a spontaneous transition from a H-mode confinement state ($H_{98} = 1.3$ at $t = 1716$ ms) to an enhanced confinement state ($H_{98} = 1.6$ at $t = 2800$ ms) is observed

while β_N and β_p are maintained constant by a feedback system that controls the power injected by neutral beams. At $t = 3200$ ms, the plasma pressure drops to $\beta_N = 1.5$ due to an $n = 1$ edge localized mode (ELM), where n is the toroidal mode number. When the β_N recovers to the feedback target, the plasma is in an even higher confinement state ($H_{98} = 1.8$ at $t = 3800$ ms). There must be a change in the plasma that allows for the improved energy confinement. The bottom panel of Figure 1 shows the electron pressure pedestal ($P_{e,ped}$). The pedestal shifts between a high pedestal ($P_{e,ped} \sim 6$ kPa) and a low pedestal state ($P_{e,ped} \sim 3$ kPa) from $t = 1600 - 2400$. After $t = 2400$, the pedestal remains in a low pedestal state. This relationship between pedestal height and ITB has also been observed in the collapse of an ITB in this scenario. When the ITB collapses and confinement degrades, the pedestal height is raised [12]. This suggests that the that the large radius ITB and the pedestal could be coupled. However, a high pedestal state with large fluctuations in β_N due to $n = 1$ ELMs has previously been observed with an ITB and high confinement [13] in this scenario suggesting that the ITB does not prohibit the high pedestal.

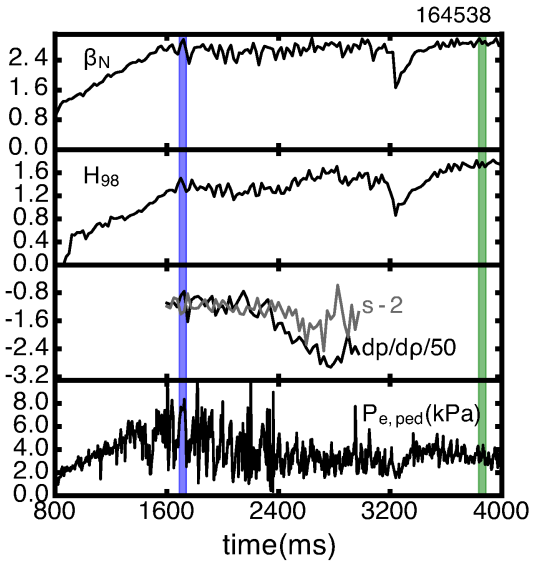

Figure 1: Time trace for discharge 164538: β_N, H_{98}, $\partial p/\partial\rho/50$ and $s - 2$ at $\rho = 0.6$ constructed from kineticEFITs, and $P_{e,ped}$.

The H-mode confinement state has a pressure profile P that is typical of an H-mode, while the enhanced confinement states have a lower pedestal and large radius ITB. The pressure profiles for the different confinement states are shown in Figure 2. The H-mode confinement state has a pedestal height of 14.5 kPa and

pedestal width of 0.08 ρ_s, where ρ_s is ρ at the last closed flux surface. The enhanced confinement states have a lower pedestal height of 8 kPa and lower pedestal width of 0.06 ρ_s. With almost twice the pedestal pressure, the H-mode confinement state has twice the pressure at $\rho \sim 0.8$ compared to the enhanced confinement ITB states. At $\rho \sim 0.6$, the pressure in the states are similar, but the ITB states have a significantly larger gradient scale length. Note that at $t = 2850$ ms, there is a tearing mode near $\rho = 0.3$, which is likely the cause of the flattening of the pressure profile in that region. To avoid complications due to the tearing mode at $t = 2850$ ms, a detailed comparison between the H-mode confinement state and the enhanced confinement state is made using the equilibria at $t = 1716$ ms and $t = 3861$ ms.

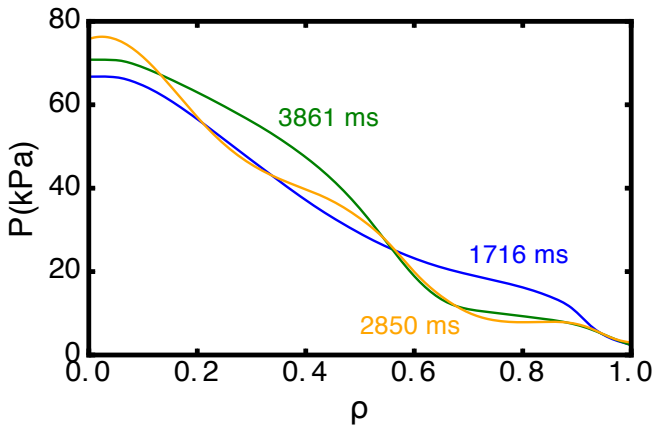

Figure 2: Pressure profiles for both H-mode confinement state (blue) and enhanced confinement ITB states (orange and green) are plotted versus ρ.

The time of the spontaneous improvement in confinement aligns well with the time of change in the mid-radius pressure gradient. Shown in the bottom panel of Figure 1, the magnitude of $\partial p/\partial \rho$ at $\rho = 0.6$ increases at the same time that the confinement begins to improve at t=2400 ms . Also shown in the bottom panel of Figure 1, s at $\rho = 0.6$ begins to change shortly after at t=2550 ms. This suggests that a change to $\partial p/\partial \rho$ enters the plasma into a positive feedback loop leading to high confinement, and s follows with the change to the bootstrap current.

To understand what role the Shafranov shift plays in sustainment of the ITB, we examine how $\alpha - s$ changes versus ρ, which is shown in Figure 3. In toroidal geometry, α and s are defined as[14]:

$$\alpha = -\frac{2\partial V/\partial\psi}{(2\pi)^2}\left(\frac{V}{2\pi^2 R_0}\right)^{1/2}\mu_0\partial P/\partial\psi$$
$$s = \frac{2V}{q}\frac{\partial q/\partial\psi}{\partial V/\partial\psi} \tag{1}$$

where, ψ is the poloidal flux, q is the safety factor, V is the plasma volume, and R_0 is the major radius. The shape of $\alpha - s$ for the enhanced confinement state is consistent with turbulence being suppressed by the Shafranov shift at large $\alpha - s$ in the core. The enhanced confinement state has strongly positive $\alpha - s$ at $\rho = 0.6$ and strongly negative $\alpha - s$ at $\rho = 0.8$. The large $\alpha - s$ in the core indicates that turbulence should be strongly suppressed in that region. The H-mode confinement state has weakly positive or negative $\alpha - s$ for the majority of the core, with a large $\alpha - s \sim 12$ near the top of the pedestal. The two most disparate points in $\alpha - s$ between the two states are at $\rho = 0.6$ and $\rho = 0.8$, and are examined in detail.

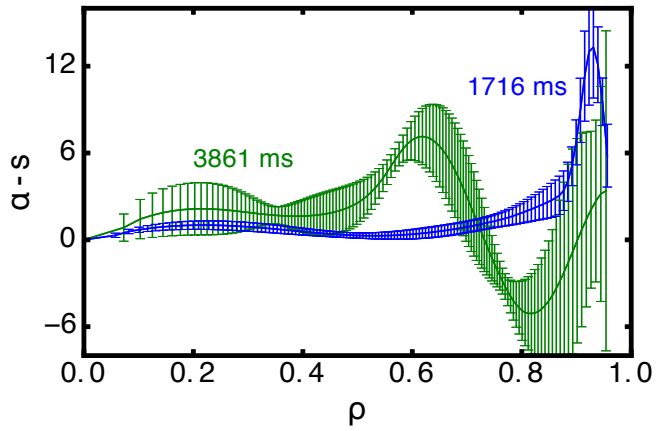

Figure 3: The $\alpha - s$ from kineticEFITs for the H-mode and enhanced confinement state are plotted versus ρ. The error is estimated by a Monte Carlo method.

Examining the relationship between experimental energy flux and $\rho = 0.6$ pressure gradient reveals the presence of a bifurcation. Figure 4 shows the experimental ion energy flux Q_i vs. $\partial p/\partial\rho$. The black line is the trajectory of discharge 164538 of Figure 1 from t=1600-3000 ms at constant $\beta_N \sim 2.7$. The red line is the trajectory of a similar discharge that had a β_N ramp up from β_N=1.4 to β_N=2.7. Putting the two discharges together, there is a clear picture of a bifurcation of ion energy transport with respect to pressure gradient, and thus with respect to the Shafranov shift which is proportional to $\partial p/\partial\rho$. At low $\partial p/\partial\rho$, Q_i increases as $\partial p/\partial\rho$ increases. However, as $\partial p/\partial\rho$ exceeds 70, the trend reverses with Q_i decreasing as $\partial p/\partial\rho$ is increased

further creating a bifurcation. In this letter, it will be shown that the bifurcation in Q_i corresponds to two simultaneous transitions. At $\rho = 0.6$, the plasma starts near the KBM instability during the H-mode state, then transitions well into the second stability of the KBM for the enhanced confinement state. At $\rho = 0.8$, the plasma starts in second stability of the KBM, then transitions through the KBM mountain to first stability. The combination of the two transitions lead to an overall improvement in confinement.

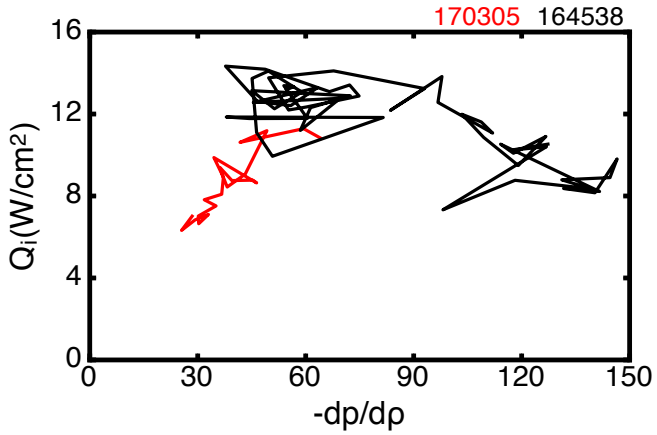

Figure 4: Experimental ion energy flux Q_i estimated by power balance is plotted vs. $\partial p/\partial \rho$ at $\rho = 0.6$

At mid-radius $\rho = 0.6$, the H-mode confinement state has a TGLF predicted turbulent energy flux of $Q_i = 1.5$ W/cm^2, where the enhanced ITB confinement state has much less predicted turbulent transport with $Q_i = 0.1$ W/cm^2. To better understand why the transport changes and how the plasma shifts between states with the shift in $\alpha - s$, intermediate states are simulated by linearly interpolating the input parameters (densities, temperatures, magnetic geometry, rotation, collisionality and Debye Length, and their respective gradients, etc) in between the two plasma states. The TGLF predicted ion energy flux is shown in Figure 5 with the enhanced confinement state highlighted in green and the H-mode confinement state in blue. As $\alpha - s$ is increased, the turbulence at $\rho = 0.6$ is stabilized by the Shafranov shift when $\alpha - s > 1$, then there are small bumps of transport at $\alpha - s = 2, 3$. To identify what mode causes the transport, the simulation is repeated electrostatically by setting $\beta_e = 0$. When $\alpha - s < 1$, the plasma is unstable to electrostatic ITG modes, then there are small bumps of transport due to an electromagnetic KBM. The plasma can transition from a H-mode confinement state to an enhanced confinement state without external manipulation, and may naturally shift to this position. This suggests that the plasma grazes the KBM instability and goes into

second stability as the plasma shifts from the H-mode confinement state to the enhanced confinement ITB state.

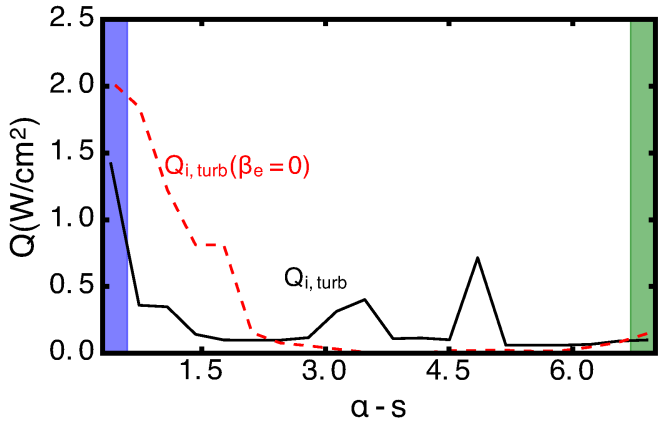

Figure 5: Turbulent ion energy flux Q_i predicted by TGLF at $\rho = 0.6$ for scan from the enhanced confinement state (highlighted in green) to the H-mode confinement state (highlighted in blue).

TGLF analysis is performed again at $\rho = 0.8$ to better understand how the transport changes at large radius. In the H-mode confinement state, the plasma is unstable to the KBM mode with a predicted turbulent energy flux of $Q_i = 2.5$ W/cm^2. The enhanced ITB confinement state has much less predicted turbulent transport with $Q_i = 0.5$ W/cm^2. Linearly interpolating between the two states which are shown in Figure 6, the turbulent energy flux rises up to $Q_i \sim 12$ W/cm^2 for the intermediate states. However, when TGLF is simulated electrostatically with $\beta_e = 0$, the mountain of transport disappears, and the Q_i decreases as $\alpha - s$ increases. This suggests that the large rise in transport in between the two states is due to an electromagnetic KBM mode, and there is a large KBM mountain of transport in between the two confinement states at $\rho = 0.8$ with the H-mode state being in second stability. Note that there are finite-n modes not simulated by TGLF that could limit the stability threshold when the plasma is second stable to KBMs.

With a large mountain of transport between the two confinement states at large radius, how the plasma transitions from second stability to first stability at $t = 2400$ ms is investigated next. At $t = 3200$ ms, the ITB is formed likely with help from the perturbation from the drop in β_N. Since TGLF predicts that the plasma can transition from the H-mode state to the ITB state without going over the large KBM mountain

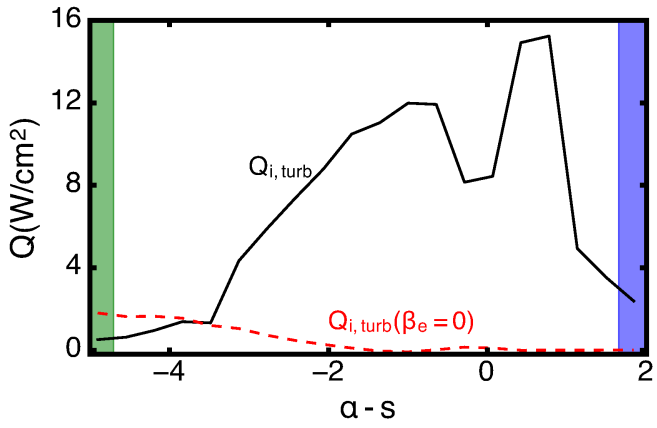

Figure 6: Turbulent ion energy flux Q_i predicted by TGLF at $\rho = 0.8$ is scanned from the enhanced confinement ITB state (highlighted in green) to the H-mode confinement state (highlighted in blue).

of transport when $\beta_e = 0$, the drop in β_N and thus β_e likely allows the plasma to transition between states without going for the KBM mountain. However, at $t = 2400$ ms, there is no large drop in β_N to help transition between states. Looking at the perturbed poloidal magnetic fields measured from Mirnov probes at the outboard midplane, shown in Figure 7, there is an $n = 1$ ELM at $t = 2360$ ms that could help transition between states. This ELM is similar to the ELM at $t = 3200$ ms, and significantly reduces the edge electron temperature (T_e) and β_e up to $\rho = 0.75$. The ELM could help ITB formation in two ways. First, it increases the the mid-radius T_e gradient, and thus increases the mid-radius pressure gradient and Shafranov shift. Second, the ELM could reduce the energy flux from the KBM without a large perturbation in β_N by temporarily reducing $\beta_e = 0$ at $\rho = 0.8$, and could allow the plasma to transition to the enhanced confinement ITB state.

In the high β_p scenario, a bifurcation of experimental transport occurs at large radius due to the Shafranov shift. The increase the pressure gradient increases the local measure of Shafranov shift α and decreases the magnetic shear s simultaneously leading to multiple positive feedback mechanisms for turbulence suppression. The plasma switches from second stability to first stability at large radius, while the mid-radius goes well into the second stability region leading to an overall improved confinement state. At large radius, there is a large KBM mountain that is passed to reach the low pedestal enhanced confinement ITB state. The plasma is helped to the first stability side of the KBM mountain at large radius from an $n = 1$ ELM, which lowers

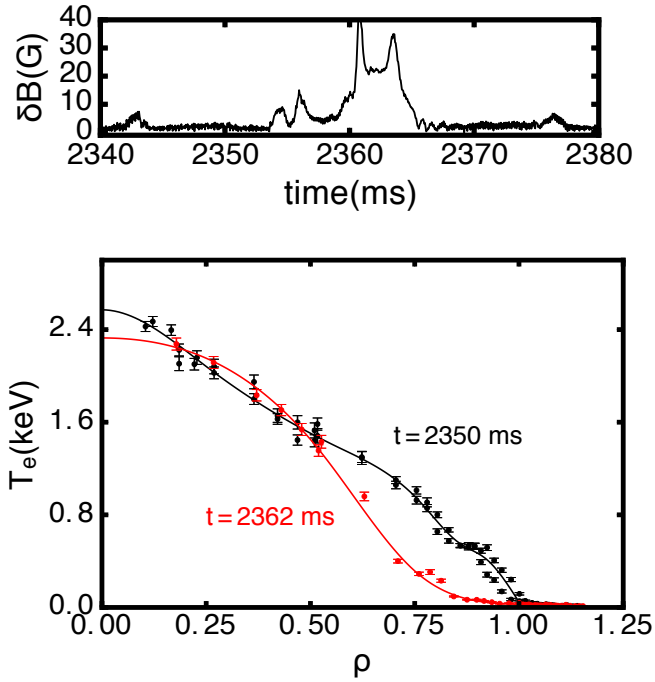

Figure 7: (Top) Magnetic field perturbation during $n = 1$ ELM, (Bottom) and electron temperature before in black and after $n = 1$ ELM in red

T_e and β_e for the plasma to pass through the mountain.

This work supported in part by the US Department of Energy (DE-FC02-04ER54698 and Cooperative Agreement DE-SC0010685), and by the National Magnetic Confinement Fusion Program of China (No.2015GB102002, 2015GB103000). DIII-D data shown in this paper can be obtained in digital format by following the links at `https://fusion.gat.com/global/D3D_DMP`. This report was prepared as an account of work sponsored by an agency of the United States Government. Neither the United States Government nor any agency thereof, nor any of their employees, makes any warranty, express or implied, or assumes any legal liability or responsibility for the accuracy, completeness, or usefulness of any information, apparatus, product, or process disclosed, or represents that its use would not infringe privately owned rights. Reference herein to any specific commercial product, process, or service by trade name, trademark, manufacturer, or otherwise does not necessarily constitute or imply its endorsement, recommendation, or favoring by the United States Government or any agency thereof. The views and opinions of authors expressed herein do not necessarily state or reflect those of the United States Government or any agency thereof.

References

[1] AR Polevoi, M Shimada, M Sugihara, Yu L Igitkhanov, VS Mukhovatov, AS Kukushkin, S Yu Medvedev, AV Zvonkov, and AA Ivanov. Requirements for pellet injection in ITER scenarios with enhanced particle confinement. *Nuclear fusion*, 45(11):1451, 2005; private communication.

[2] C Bourdelle, GT Hoang, X Litaudon, CM Roach, T Tala, International ITB Database Working Group, et al. Impact of the α parameter on the microstability of internal transport barriers. *Nuclear fusion*, 45(2):110, 2005.

[3] Michael A Beer, GW Hammett, G Rewoldt, EJ Synakowski, MC Zarnstorff, and W Dorland. Gyrofluid simulations of turbulence suppression in reversed-shear experiments on the Tokamak Fusion Test Reactor. *Physics of Plasmas (1994-present)*, 4(5):1792–1799, 1997.

[4] EJ Synakowski, SH Batha, MA Beer, MG Bell, RE Bell, RV Budny, CE Bush, PC Efthimion, GW Hammett, TS Hahm, et al. Roles of electric field shear and shafranov shift in sustaining high confinement in enhanced reversed shear plasmas on the tftr tokamak. *Physical review letters*, 78(15):2972, 1997.

[5] M Kikuchi. Steady state tokamak reactor based on the bootstrap current. *Nuclear fusion*, 30(2):265, 1990.

[6] T Fujita, Y Kamada, S Ide, S Takeji, Y Sakamoto, A Isayama, T Suzuki, T Oikawa, T Fukuda, et al. Sustainment of high confinement in jt-60u reversed shear plasmas. *Nuclear fusion*, 42(2):180, 2002.

[7] Jorg Hobirk, Robert C Wolf, O Gruber, A Gude, Sibylle Günter, Bernd Kurzan, Marc Maraschek, Patrick J McCarthy, Hans Meister, Arthur G Peeters, et al. Reaching high poloidal beta at greenwald density with internal transport barrier close to full noninductive current drive. *Physical review letters*, 87(8):085002, 2001.

[8] AM Garofalo, X Gong, BA Grierson, Q Ren, WM Solomon, EJ Strait, MA Van Zeeland, CT Holcomb, O Meneghini, SP Smith, et al. Compatibility of internal transport barrier with steady-state operation in the high bootstrap fraction regime on DIII-D. *Nuclear Fusion*, 55(12):123025, 2015.

[9] G.M. Staebler. Transport barriers in bootstrap driven tokamaks. *To be published in Physics of Plasmas.*

[10] GM Staebler, JE Kinsey, and RE Waltz. A theory-based transport model with comprehensive physics. *Physics of Plasmas (1994-present)*, 14(5):055909, 2007.

[11] J Candy and RE Waltz. An eulerian gyrokinetic-maxwell solver. *Journal of Computational Physics*, 186(2):545–581, 2003.

[12] AM Garofalo, XZ Gong, SY Ding, J Huang, J McClenaghan, CK Pan, J Qian, QL Ren, GM Staebler, J Chen, et al. Joint diii-d/east research on the development of a high poloidal beta scenario for the steady state missions of iter and cfetr. *Plasma Physics and Controlled Fusion*, 60(1):014043, 2017.

[13] Chengkang Pan, Gary M Staebler, Lang L Lao, Andrea M Garofalo, Xianzu Gong, Qilong Ren, Jonathan McClenaghan, Guoqiang Li, Siye Ding, Jinping Qian, et al. Investigation of energy transport in diii-d high-β p east-demonstration discharges with the tglf turbulent and neo neoclassical transport models. *Nuclear Fusion*, 57(3):036018, 2017.

[14] RL Miller, MS Chu, JM Greene, YR Lin-Liu, and RE Waltz. Noncircular, finite aspect ratio, local equilibrium model. *Physics of Plasmas*, 5(4):973–978, 1998.